HHS Public Access

Author manuscript

Int J Min Sci Technol. Author manuscript; available in PMC 2019 February 19.

Published in final edited form as:

Int J Min Sci Technol. 2019 January ; 29(1): 105–111. doi:10.1016/j.ijmst.2018.11.008.

Development of a fault-rupture environment in 3D: A numerical tool for examining the mechanical impact of a fault on underground excavations

Bo-Hyun Kim* and **Mark K. Larson**

Spokane Mining Research Division, CDC/NIOSH, Spokane, WA 99207, United States

Abstract

While faults are commonly simulated as a single planar or non-planar interface for a safety or stability analysis in underground mining excavation, the real 3D structure of a fault is often very complex, with different branches that reactivate at different times. Furthermore, these branches are zones of nonzero thickness where material continuously undergoes damage even during interseismic periods. In this study, the initiation and the initial evolution of a strike-slip fault was modeled using the FLAC3D software program. The initial and boundary conditions are simplified, and mimic the Riedel shear experiment and the constitutive model in the literature. The FLAC3D model successfully replicates and creates the 3D fault zone as a strike-slip type structure in the entire thickness of the model. The strike-slip fault structure and normal displacement result in the formation of valleys in the model. Three panels of a longwall excavation are virtually placed and excavated beneath a main valley. The characteristics of stored and dissipated energy associated with the panel excavations are examined and observed at different stages of shear strain in the fault to evaluate bump potential. Depending on the shear strain in the fault, the energy characteristics adjacent to the longwall panels present different degrees of bump potential, which is not possible to capture by conventional fault simulation using an interface.

Keywords

3D fault zone; Strike-slip fault; FLAC3D; Bump potential; Energy characteristics

1. Introduction

This paper is part of an effort by the National Institute for Occupational Safety and Health (NIOSH) to identify risk factors associated with bump-prone potential in highly stressed ground conditions. More specifically, this paper reports an exploratory effort with an unconventional approach using a numerical tool to try to better understand a possible scenario where bump risk might be increased—that is, a scenario involving a strike-slip

*Corresponding author. ljn0@cdc.gov (B.-H. Kim).

fault. The objective is to assess whether a numerical tool might be useful or practical in forecasting bump potential associated with a strike-slip fault for a typical structural geologic setting.

The highly anisotropic characteristics of coal seams that result from geologic structures when mining takes place, such as cleats, bedding, faults, and spatial redistribution of induced stress in coal pillars, cause many uncertainties that affect safety. Dynamic failure in coal mines, known as “bumps”, is one of the most challenging and persistent engineering problems associated with coal mining in highly stressed conditions. These events occur when stresses in a coal pillar, used for support in underground workings, exceed the critical strength of the pillar, causing the pillar to rupture without warning. These events can be exceptionally violent, ejecting coal and rock with explosive force. These types of events have been documented for well over 100 years within the American underground coal mining industry. During this time, mining practices and support technologies have evolved considerably, resulting in an overall decrease in the rate of dynamic failure-related injuries and fatalities. However, they do continue to occur. Fig. 1 presents the number and rate of fatalities for the last 10 years in underground coal mining show that the trend is still highly fluctuant. Fig. 2 shows that, from 1983 to 2014, there were nearly 400 cases of reportable dynamic failure accidents in coal and nonmetal mines, resulting in 20 fatalities, 155 lost-time accidents, and an estimated 48,000 lost man-hours [1]. However, a continuous effort to better understand the dynamic failure mechanism in coal mines is still required in order to make further improvements in preventing bump-related fatalities in underground coal mining.

The risk associated with faults/fault zones and coal bumps has been acknowledged by several researchers in the literature. Mauck [2] and Peperakis [3] mention the risk of bumps with regard to the proximity of mining operations to faults. Some describe the role of faults in stress concentration [3–7], thus causing conditions with increased bump risk. Others specifically mention fault slip and the resulting release of energy associated with bumps [3,5–8]. Iannacchione and Zelanko [9] mention the role of geologic structure, including displacement faults, to concentrate stress and control the caving and heaving characteristics of strata. The risk of bumps associated with faults is well established; however, the specific mechanisms that cause bumps may not be well understood. For that reason, a numerical tool that involves a new approach is used in this study to examine the problem and assess the potential to identify the risk of bumps associated with strike-slip faults.

Specifically in this study, bump potential near a fault zone associated with a longwall mining excavation is evaluated with respect to the different stages of shear strain in the fault using a new numerical modeling technique. The influence of stored and dissipated energy, due to the fault deformation and the timing of long-wall excavation on the potential for a bump adjacent to the fault, is also investigated using the numerical model.

Faults, in general, are simulated as a single planar or non-planar interface by a numerical tool for a safety or stability analysis in underground mining excavation. However, the real 3D structure of a fault is commonly very complex, with different branches that reactivate at

different times. Furthermore, these branches are zones of non-zero thickness where material continuously undergoes damage even during interseismic periods [11].

In this study, FLAC3D [12] is used to simulate the initiation and the initial evolution of a strike-slip fault. The initial and boundary conditions are simplified and mimic the Riedel shear experiment and the methodologies introduced by Chemenda et al. [11]. The successful replication of Chemenda's model created a valley in the FLAC3D model due to the fault's formation by the shearing. Three longwall panels are excavated beneath the central valley that will be discussed in detail later. It is assumed, in agreement with Kim et al. [13], that the risk of bumps would increase proportionally to the ratio of elastic energy to dissipated plastic energy. The elastic energy is stored in the rock mass due to the panel excavations. The release of this retained energy is then subject to stress redistribution due to the fault deformation and excavation of the longwall panels in the model. The release of plastic energy, by contrast, dissipates through the rock mass at the ribs, roof, and floor adjacent to the mine entry. In order to investigate and quantify the risk posed by this possible imbalance, the energy is calculated using FLAC3D so that the elastic strain energy and dissipated plastic energy can be tracked for given zones in the model.

This paper describes common approaches for a fault-slip analysis. The approach for FLAC3D modeling, including assumptions and conditions, is also described. Methodologies appropriate to evaluate the bump potential due to longwall mining excavation are explained and demonstrated by means of the modeling technique.

2. Numerical approach for fault-slip analysis

At present, a number of numerical simulation methods have been developed in a variety of fields to analyze physical phenomena, such as elastic wave propagation, ground motion induced by seismic waves, rock mass behavior, and crack propagation within intact materials. Cappa and Rutqvist [14] employ the finite difference method to simulate the behavior of geological discontinuities. Alber et al. [15] evaluate fault-slip tendency by carrying out static analysis using the finite element method. In the field of geophysics, Oglesby and Mai [16] simulate dynamic shear rupture as a source of an earthquake that could occur on the North Anatolian Fault system in the Sea of Marmara, Turkey, with a large-scale numerical model. Potvin et al. [17] and Sjöberg et al. [18] use a distinct element method in order to simulate fault-slip that occurs along geological structures in underground mines. However, all these analyses considered the fault in the numerical model as a single planar or non-planar interface, ignoring the fault's specific shape or thickness for the purpose of simplification.

Chemenda et al. [11] demonstrate that they were able to properly model the initiation and initial evolution of the complex structure in a strike-slip fault by using a constitutive model that takes into account the hardening of a plastic modulus with inelastic straining. They also used "softer" boundary conditions by prescribing tractions instead of velocities. In an attempt to reproduce the results of their study, we implemented their constitutive model in FISH (a programming language available in FLAC3D) and calibrated an in-house model to

replicate the same behavior. We also implemented the same boundary conditions for strike-slip conditions.

3. Replication and development of the strike-slip fault in FLAC3D

To replicate and develop a strike-slip fault in FLAC3D, it is necessary to study the 3D fault structure during the initial evolution of the fault (i.e., initial elastic deformation followed by damage propagation to form a flower-like structure in the cross section). To do this, Chemenda et al. [11] construct a model using FLAC3D and apply shear forces at the boundaries in plain view. During the initial stages of the model evolution, the response is purely elastic. At a certain stage, the inelastic deformation starts at the surface in the longitudinal axial area. The inelastic zone thickens and rapidly widens in the lateral axis of the model. At some point, the damage due to inelastic deformation starts at the model bottom. In the next stage, a dense set of parallel deformation localization bands of incipient faults forms. The whole band set first evolves uniformly, and then a sort of band selection process is observed. Finally, the entire thickness of the layer is affected, forming a flower-like structure in the cross section, as shown in Fig. 3(a). Fig. 3(b) implies that these are normal or normal shear faults whose activity results in the formation of 100-m-deep valleys.

In order to replicate the strike-slip model developed by Chemenda et al. [11], a FLAC3D model with dimensions of 50,000 m (W) × 5000 m (H) × 100,000 m (L) is constructed. Each zone size is set up to be approximately 300 m. The generalized Hoek-Brown model with strain-softening behavior is chosen as the failure criterion for this simulation [12]. Some generic mechanical properties for the rock mass are selected for the model to achieve the objective of examining whether a template for the physically formed strike-slip fault in the 3D model would be suitable to study the risk potential for bumps. The mechanical properties are shown in Table 1.

The strain-softening behavior of the strength via the Hoek-Brown constants are modeled by a linear reduction to the critical shear strain as a function of the geological strength index (GSI). The inhomogeneous strength of the rock mass is also taken into account to promote stress localization. The FLAC3D model is subjected to a gravity force that generates the initial stresses, characterized by the vertical stress defined by the unit weight and the depth. Along the *y*-parallel vertical boundaries, roller conditions are applied. A kinematic condition is imposed along the *y*-normal boundaries. By means of implementing the boundary and loading conditions introduced by Chemenda et al. [11], the movement of nodes at the front and back faces are slaved to the corresponding nodes at the mid-section (at $L/2$). A shear stress, which increases progressively during deformation, is applied to the bottom of the model, which is fixed in the z-direction. The load is incrementally applied so that inertial effects are minimized.

Fig. 4 illustrates the construction of the FLAC3D model and how the shear stress loading is applied on the boundaries (Fig. 4(a)), along with the FLAC3D model after the deformation resulting from the shear stress loading (Fig. 4(b)).

Fig. 5 Simulated faults and shear zones and deformation in the model shows that the replication of Chemenda's approach is successfully accomplished using the methodologies explained. Fig. 5(a) shows that a series of valleys are formed in the model by the shear stress loading in terms of the contours of shear strain. Fig. 5(b) illustrates the iso-blocks of shear strain plotted with partially transparent colors. The iso-block shows contours or iso-surfaces of zone-based values of shear strain on zone faces. Zone faces are plotted if the value of the zone on either side of the face crosses the iso-value specified [12]. In this case, the iso-value is 1% shear strain. The iso-block can represent a fault zone that is physically deformed due to the shear stress with non-zero thickness and a certain shape, which appears to be very different compared to the modeled results of an interface simulated as a single planar or non-planar structure in a numerical model. Fig. 5(c) shows that valleys are created by a fault system formation due to the shear stress loading.

4. Excavation of longwall panels

As the next step, a generic configuration of three longwall panels is placed beneath the central valley at the middle of the model. The panels are excavated one by one in order to investigate any change of the energy state, according to the deformation of the fault and panel excavations.

Since the FLAC3D model is constructed with relatively coarse elements approximately 300 m in size along one side, it is not appropriate to build an underground excavation in the model for the investigation with no modification of the size of the element. Therefore, the region of interest for this study is densified—that is, zones are divided into smaller zones but limited in extent, so a smooth transition of stress calculation is achieved. This is accomplished by limiting the change in the size of adjacent elements to one order of magnitude. Two internal densified regions are designed as a shell and generated in the middle of the model, as shown in Fig. 6(a). The outer shell is built with 30-m elements as illustrated in Fig. 6(b). The inner shell—mainly for investigating change in the energy state associated with the panel excavations—is created inside the outer shell and has an element size of 3 m, as presented in Fig. 6(c). In the inner shell, we generate and place three panels representing a longwall mining excavation. The dimensions of the panels are 120 m (W) × 6 m (H) × 500 m (L), and the pillars between the panels are 30 m wide. The depth of the panels is approximately 1500 m below the top surface of the model. Because the size of the excavations is relatively small compared to the whole model, the panels were excavated as a whole, panel by panel, and not gradually.

5. Energy ratio results and discussion

Elastic strain energy and dissipated plastic energy can be tracked if zones in the model have an assigned mechanical constitutive model, which is the case in this model. The FLAC3D model uses an incremental solution procedure: the equations of motion at the gridpoints and the stress-strain calculations at the zones are solved at every timestep, progressing toward equilibrium. In the stress-strain equations, the incremental change in energy components is determined and accumulated as the system attempts to reach equilibrium. Energy is

dissipated through plastic work as the zones undergo irreversible deformation. The strain in any zone can be divided into elastic and plastic parts [12].

Kim et al. [13] report that the individual ratio of plastic dissipated energy in terms of the intensity of energy release at the different locations can be characterized and quantified by multiple regression. From that analysis, the shear strength of the adjacent contacts in terms of internal friction angle is, in general, the most critical parameter contributing to the dissipation of plastic energy. This is particularly important near the gateroads. In this study, we compare two different states of the fault physically developed by the shear stress loading —that is, two different amounts of applied shear stress. One state represents a relatively small amount of fault deformation: 0.1% shear strain as measured on the fault plane. The other state represents a relatively larger amount of fault deformation: 10% shear strain observed on the fault plane. This is accomplished by continuing to load beyond the state having 0.1% shear strain along the fault. Because the induced shear strain along these faults is not constant, the size and thickness of the faults eventually become non-uniform. These conditions cannot be simulated explicitly by a single planar or non-planar interface. Therefore, these two states in fault deformation, 0.1% shear strain versus 10% shear strain, are expected to show different conditions in terms of stored and dissipated energy, particularly with respect to the longwall panel excavations.

Bigarre et al. [19] indicate that seismic energy associated with rockbursts (i.e., bumps) in a deep coal mine at a depth reaching 1100 m varies around 10^8 to 10^9 J, with an associated Richter ranging from 2.2 to 3. Fig. 7 shows the results of the plastic dissipated energy in the vicinity of the faults when each of the panels are excavated. The three figures in the left column present the distribution of the plastic dissipated energy around the panels where the fault induces smaller shear strain. The three figures in the right column show the plastic dissipated energy around the panels where the fault induces larger shear strain. The hotter color in the roof, floor, and pillar indicates that the dissipated plastic energy is greater than 10^8 J. The fault movement at the bottom of the valley is the main cause of the highly dissipated energy concentrated under the second panel of the floor. The intensity of the plastic dissipated energy around the longwall panels, particularly in the pillars, looks more severe when the panels are excavated in the vicinity of the fault, induced by the relatively larger deformation. The most likely interpretation is that bump risk would increase as the panels are excavated when the adjacent fault induces a relatively larger deformation in terms of shear strain.

Kim and Larson [20] find that conditions develop in their models where the ratio of potential energy to dissipated plastic energy in the vicinity of excavations varies, according to conditions of geometry and material properties. They surmise that this ratio might be used as a good indicator of the risk of bumps. Fig. 8 presents the ratio of the elastic stored energy to the plastic dissipated energy after mining each of the longwall panels. Fig. 8 in the left column presents the change of the energy ratio around the panels where the fault induces smaller shear strain (about 0.1%). Fig. 8 in the right column shows the energy ratio around the panels where the fault induces larger shear strain (about 10%). The hotter color in the roof and floor indicates the energy ratio of more than 4, which means a significant amount of the elastic energy still remains above the roof and below the floor of the panel after the

excavation. Since the energy ratio appears to be more significant in the left column in the figure, bump potential would be greater after completion of the panel excavation when the adjacent fault induces a relatively smaller shear strain.

6. Concluding remarks

In this study, the FLAC3D model successfully replicates and creates a 3D fault zone as a strike-slip type structure by means of simplifying and mimicking the initial and boundary conditions based on the methodologies proposed by Chemenda et al. [11]. This model can simulate and be used to investigate fault behavior and the effect on mining excavations more realistically by considering the fault size and thickness instead of using the common approach of modeling faults as a single planar or non-planar interface. The generic configurations of three longwall panels are embedded in the vicinity of the central valley due to the fault formation. The panels are excavated one by one in order to investigate a change of the energy state, according to the deformation of the fault and panel excavations.

The following are the results of the fault-rupture model and calculation of the energy component associated with the longwall panel excavations, using the FLAC3D modeling technique and considering the conditions and methodologies described in this paper:

1. The iso-block in the model can represent a fault zone that is physically deformed due to the shear stress with non-zero thickness and a certain shape, which appears as a feature quite different from that of a fault structure simulated with a single planar or non-planar interface in a numerical model.
2. Bump potential seems to increase if the panels are excavated after the adjacent fault induces a relatively larger shear strain deformation. This risk is indicated by the large amounts of dissipated plastic energy near the excavations.
3. Bump potential would be high if the panels are excavated when the adjacent fault induces a relatively smaller shear strain. This risk is indicated by the large ratio of elastic energy to dissipated plastic energy, which results from mining.
4. A better understanding of the risk of bumps is a critical step in improving miner safety in coal mines. Using the proposed methodology beyond evaluating bump potential in a highly stressed longwall coal mine as a function of structural geologic characteristics is a necessary step to accomplish the eventual elimination of coal pillar bursts and bump-related worker injuries and fatalities.
5. The objective of this study was accomplished in that an unconventional technique shown in the literature was reproduced using a numerical model to represent the mechanics of a strike-slip fault, and energy calculations were then used to forecast bump potential. However, no calibration can be demonstrated at this moment. Therefore, further effort on calibration with a real longwall coal mining case will definitely be required. In addition, developing a generalized template that can simulate any faulting regime, including cases involving two components, such as normal and strike-slip or reverse and strike-slip faults, might be necessary for future work.

Acknowledgement

The authors greatly appreciate the help of Dr. Varun at the Itasca Consulting Group, Inc., Minneapolis, MN, who made this work possible.

References

[1]. MSHA. MSHA accident, illness and injury and employment self-extracting files (part 50 data), U.S. Departmenr of Labor, Mine Safety and Health Administration (MSHA), Office of Injury and Employment Information; 2015.

[2]. Mauck HE. Coal mine bumps can be eliminated. Mining Eng 1958;10:923.

[3]. Peperakis J Mountain bumps at the sunnyside mines. Mining Eng 1958;10:982–6.

[4]. Agapito JFT, Goodrich RR. Five stress factors conducive to bumps in Utah, USA, coal mines In: Proceedings: 19th international conference on ground control in mining. Morgantown, WV: August 8–10, 2000. Morgantown, WV: West Virginia University; 2000 p. 93–100.

[5]. Maleki H, White B. Geotechnical factors influencing violent failure in U.S. mines In: Proceedings: international symposium on rock support—applied solutions for underground structures. Lillehammer, Norway: June 22–25, 1997. Oslo, Norway: Norwegian Society of Chartered Engineers; 1997 p. 208–21.

[6]. Boler FM, Billington S, Zipf RK. Seismological and energy balance constraints on the mechanism of a catastrophic bump in the Book Cliffs Coal Mining District, Utah, USA. Int J Rock Mech Min Sci 1997;34:27–43.

[7]. Mark C, Gauna M. Evaluating the risk of coal bursts in underground coal mines In: Proceedings: 34th international conference on ground control in mining. Morgantown, WV: July 28–30, 2015. Morgantown, WV: West Virginia University; 2015 p. 47–53.

[8]. Rice GS. Bumps in coal mines—theories of causes and suggested means of prevention or of minimizing effects. Trans Am Inst Mining Metall Eng 1936;119:11–39.

[9]. Iannacchione AT, Zelanko JC. Occurrence and remediation of coal mine bumps: A historical review In: Maleki H, Wopat PF, Repsher RC, Tuchman RJ, editors. Proceedings: mechanics and mitigation of violent failure in coal and hard-rock mines. U.S. Department of the Interior, Bureau of Mines (USBM); 1995 p. 27–67.

[10]. NIOSH. Historical mine disasters, National Institute for Occupational Safety and Health (NIOSH); 2017.

[11]. Chemenda AI, Cavalié O, Vergnolle M, Bouissou S, Delouis B. Numerical model of formation of a 3-D strike-slip fault system. C R Geosci 2016;348:61–9.

[12]. Itasca Consulting Group. FLAC3D: Fast Langrangian Analysis of Continua in 3D. ver. 6.0, Minneapolis, MN: Itasca Consulting Group, Inc.; 2018.

[13]. Kim BH, Larson MK, Lawson HE. Applying robust design to study the effects of stratigraphic characteristics on brittle failure and bump potential in a coal mine. Int J Min Sci Technol 2018;28:137–44. [PubMed: 29416902]

[14]. Cappa F, Rutqvist J. Modeling of coupled deformation and permeability evolution during fault reactivation induced by deep underground injection of CO2. Int J Greenhouse Gas Control 2011;5:336–46.

[15]. Alber M, Fritschen R, Bischoff M, Meier T. Rock mechanical investigations of seismic events in a deep longwall coal mine. Int J Rock Mech Min Sci 2009;46:408–20.

[16]. Oglesby DD, Mai PM. Fault geometry, rupture dynamics and ground motion from potential earthquakes on the North Anatolian fault under the sea of marmara. Geophys J Int 2012;188:1071–87.

[17]. Potvin Y, Jarufe J, Wesseloo J. Interpretation of seismic data and numerical modelling of fault reactivation at El Teniente, Reservas Norte sector. Mining Technol 2010;119:175–81.

[18]. Sjöberg J, Perman F, Quinteiro C, Malmgren L, Dahnér-Lindkvist C, Boskovic M. Numerical analysis of alternative mining sequences to minimise potential for fault slip rockbursting. Mining Technol 2012;121:226–35.

[19]. Bigarre P, Tinucci J, Slimane KB. 3-Dimensional modeling of fault-slip rockbursting. In: Rockbursts and seismicity in mines 93: proceedings of the 3rd international symposium on rockbursts and seimicity in mines Kingston, Ontario, Canada: August 16–18, 1993 Rotterdam: A. A. Balkema; 1993 p. 315–9.

[20]. Kim BH, Larson MK. Evaluation of bumps-prone potential regarding the spatial characteristics of cleat in coal pillars under highly stressed ground conditions. In: Proceedings, 51st U.S. rock mechanics/geomechanics symposium San Francisco: June 25–28, 2017 Alexandria, VA: American Rock Mechanics Association (ARMA); 2017 p. 8.

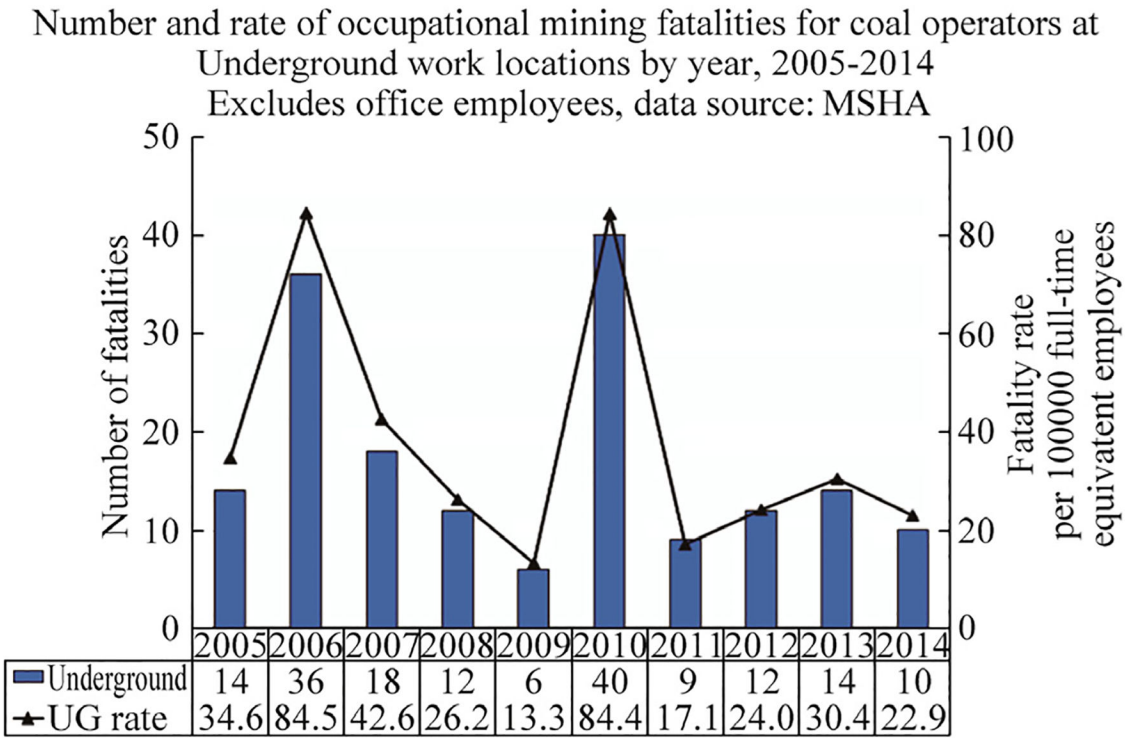

Fig. 1.

Number and rate of occupational mining fatalities for coal mining operators at underground work locations by year from 2005 through 2014 [10].

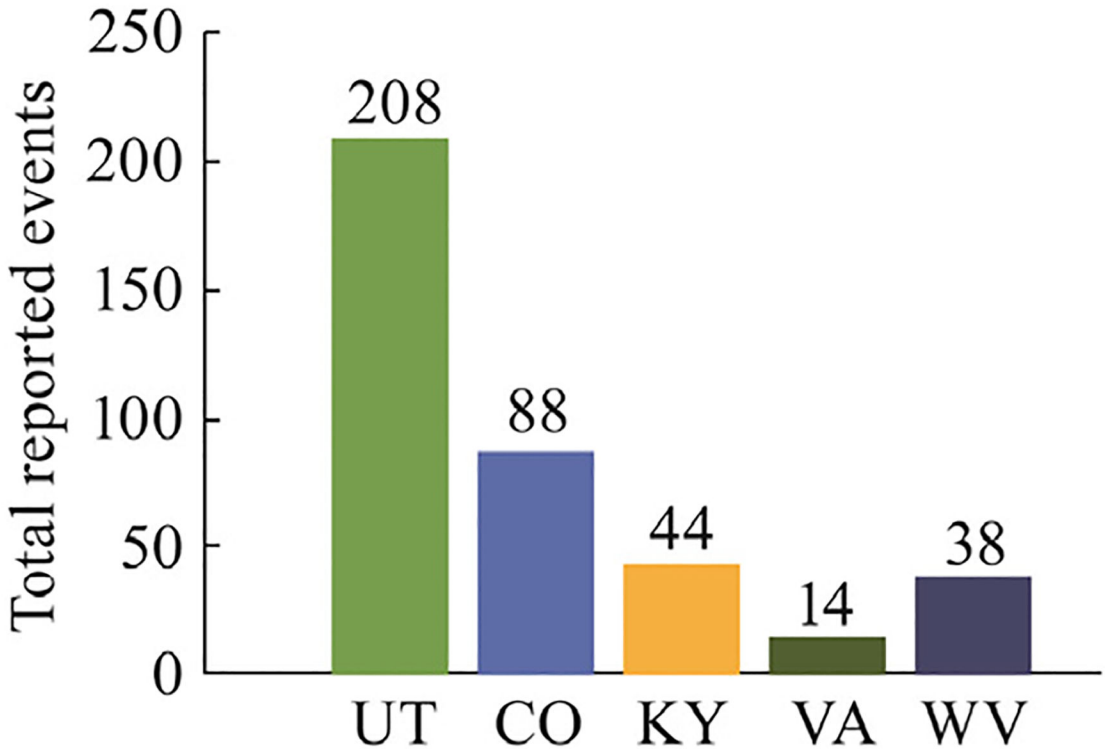

Fig. 2.
Overall geographic breakdown of MSHA-reportable dynamic failure events, 1983–2014.

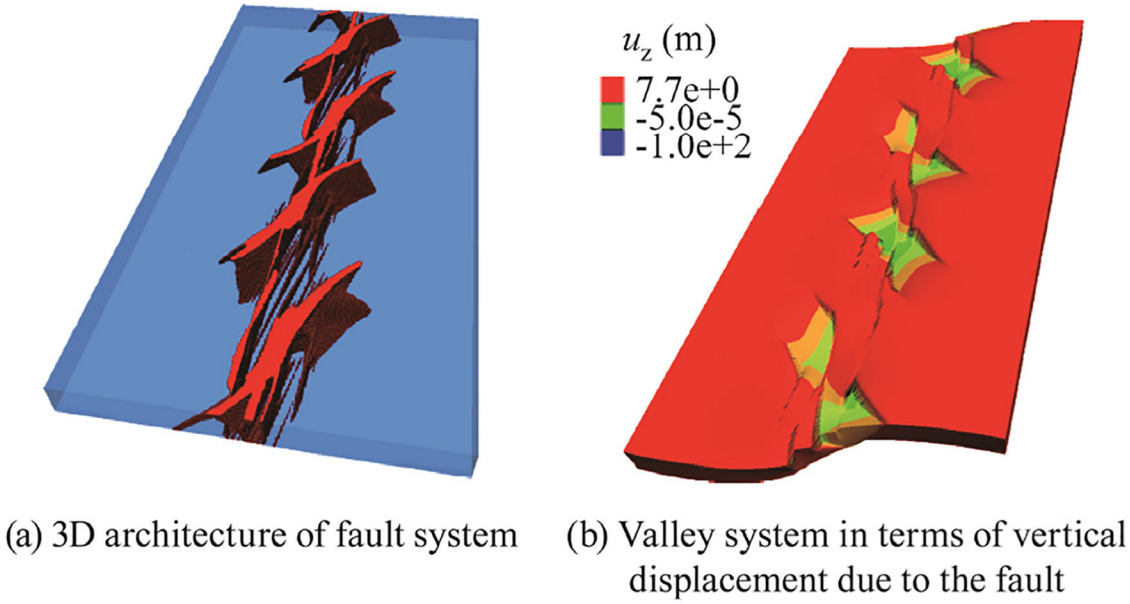

Fig. 3.
Fault system and the induced displacement simulated by Chemenda et al. [11].

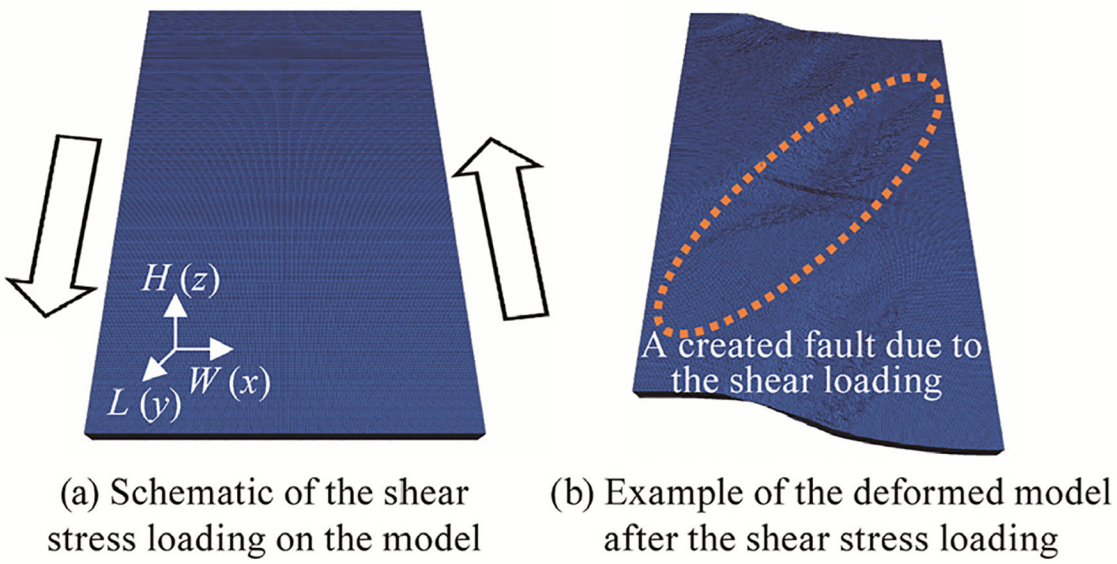

Fig. 4.
Boundary conditions for the numerical model and its effect as presented in the model.

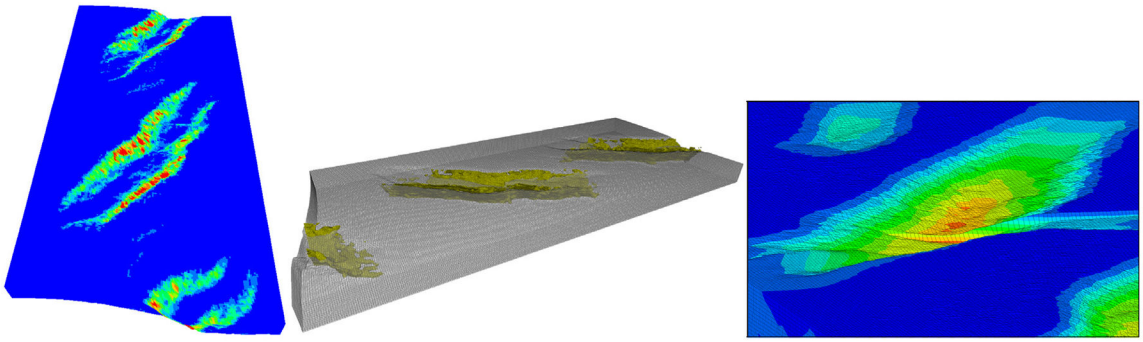

(a) Replicated fault system (b) Fault planes indicated by the iso-blocks in a 3D view (c) Created valleys due to the fault plotted as vertical displacement contours

Fig. 5.
Simulated faults and shear zones and deformation in the model.

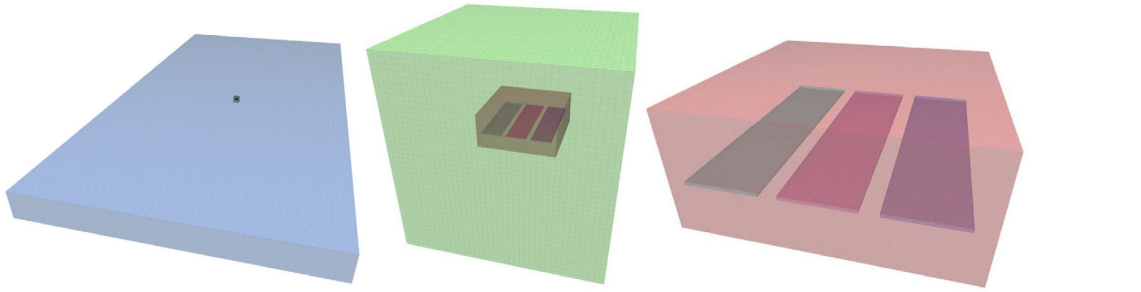

(a) Densified two shells inside the FLAC3D model (b) Densified outer shell (c) Densified inner shell embedding the longwall panels

Fig. 6.

The layout of the longwall panels associated with zone densification in the model.

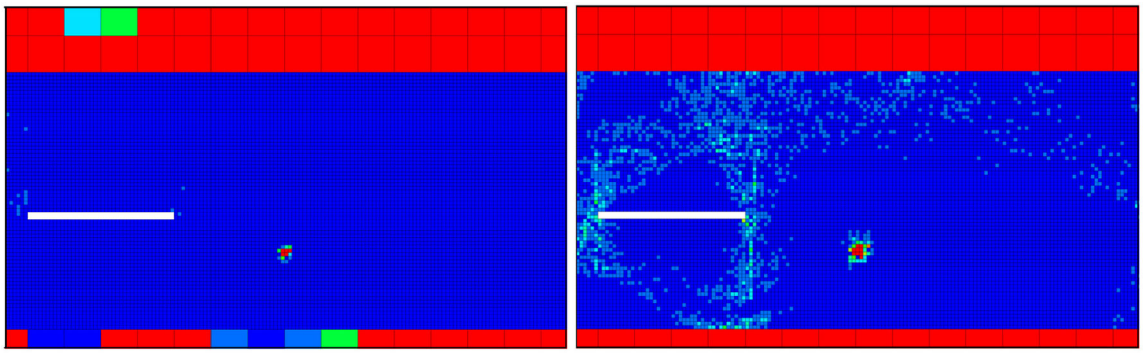

(a) After panel 1 excavation (left: small shear strain on the fault; right: large shear strain on the fault)

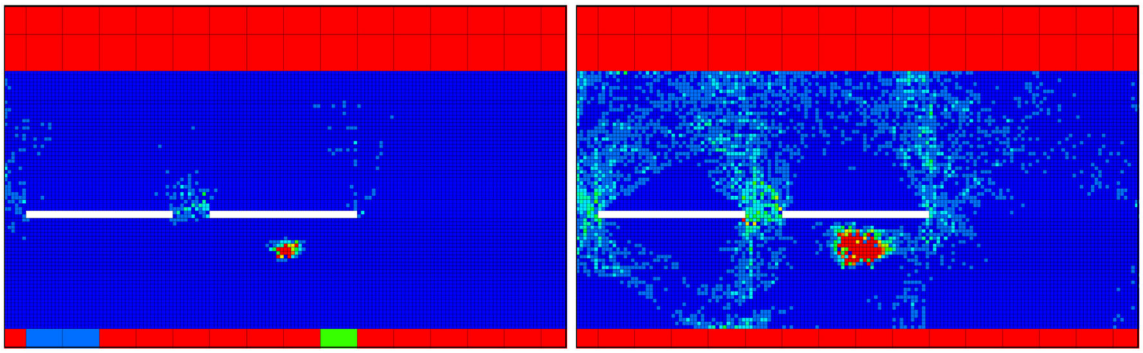

(b) After panel 2 excavation (left: small shear strain on the fault ; right: large shear strain on the fault)

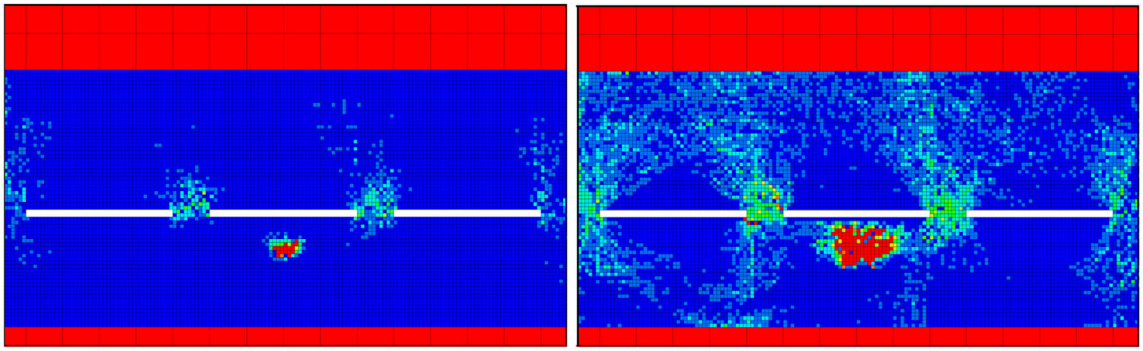

(c) After panel 3 excavation (left: small shear strain on the fault; right: large shear strain on the fault)

Fig. 7.

Contours of plastic dissipated energy after excavation of each panel at the different stages of the fault.

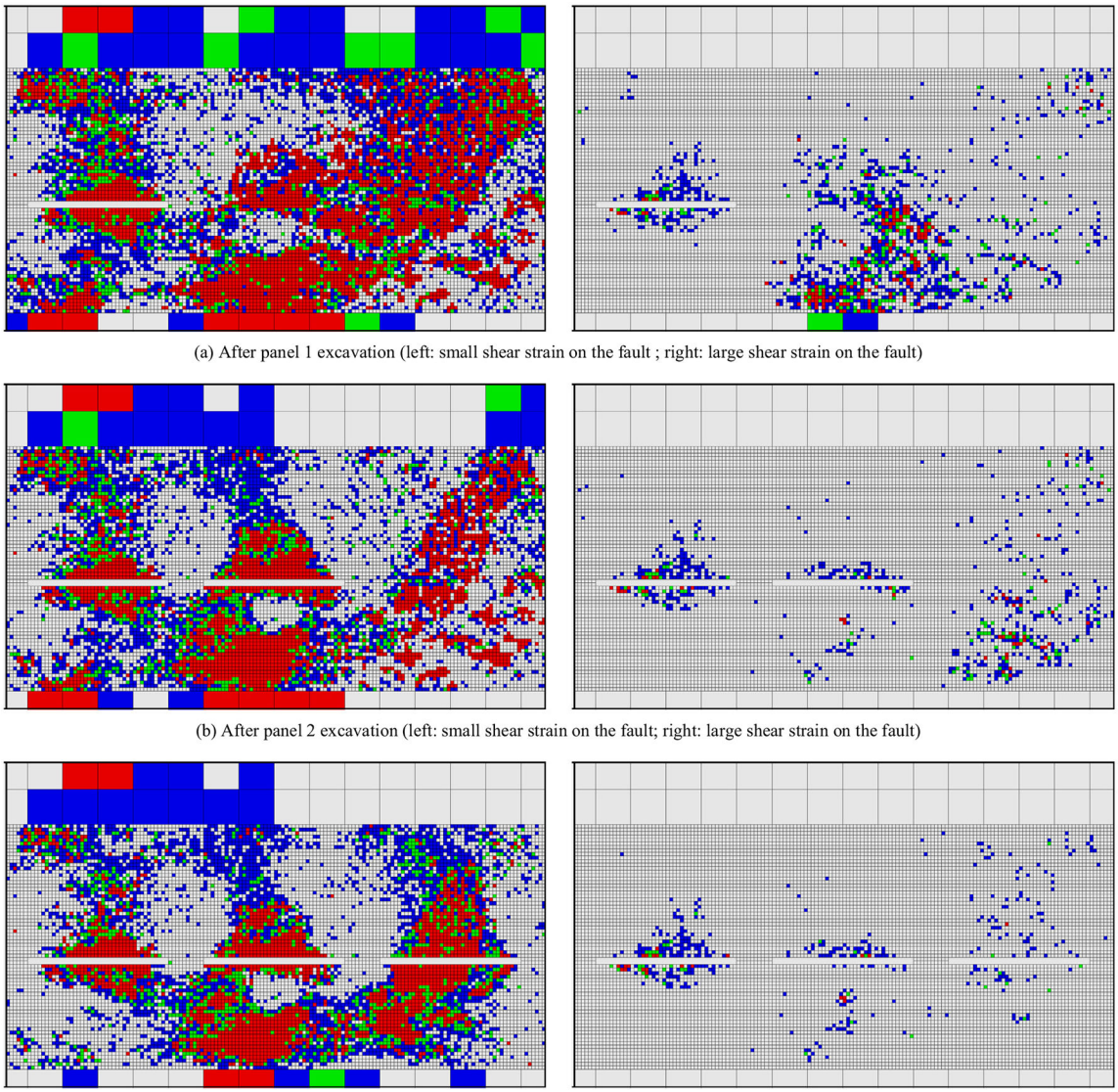

(a) After panel 1 excavation (left: small shear strain on the fault ; right: large shear strain on the fault)

(b) After panel 2 excavation (left: small shear strain on the fault; right: large shear strain on the fault)

(c) After panel 3 excavation (left: small shear strain on the fault; right: large shear strain on the fault)

Fig. 8.

Ratio of elastic stored to plastic dissipated energy after excavation of each panel at the different stages of the fault.

Table 1

Determination of the levels of the confinement for the confined compressive test.

Input parameter	Value
Unit weight (MN/m^3)	0.027
Intact Young's modulus (GPa)	50
Poisson's ratio	0.25
Geological strength index	65
Intact Hoek-Brown constant m_i	35
Intact unconfined compressive strength (MPa)	57 ± 16